Field-induced transitions and spatial chaos in the classical *XY* spin chain

Radha Balakrishnan and Mitaxi Mehta
The Institute of Mathematical Sciences, CIT Campus, Chennai 600 113, India
(Received 19 August 1998; revised manuscript received 14 October 1999)

We study the lowest-lying excitation of a classical ferromagnetic *XY* spin chain, in the presence of a symmetry breaking magnetic field. Extremizing the energy of this system leads to a two-dimensional nonlinear map, whose allowed phase space shrinks with increasing field in a nontrivial manner. The orbits of the map represent the set of extremum energy spin configurations. For each field, we compute the energy of the members of this set and find the lowest energy among them, excluding the obvious ground state configuration with all spins parallel along the field direction. This state turns out to be the unstable fixed point of the map. We show that up to a certain (primary) critical field, a separatrixlike 2π soliton configuration is the lowest-energy excitation, with an energy very close to the ground state energy. For any field beyond this critical field, the soliton disappears and lowest excitation is a librational configuration corresponding to the outermost orbit in the phase plot at that field. Further, its energy is found to be much higher than the ground state energy, leading to a sharp jump in the difference in energy between the former and the latter at this field. With further increase in the field, sharp jumps in the excitation energy arise at certain secondary critical fields as well. We show that these appear when the corresponding spin configurations become commensurate. This complex behavior of the energy is interpreted and its effect on the magnetization and static susceptibility of the system is also studied.

PACS number(s): 05.45.−a

I. INTRODUCTION

During the past three decades, a considerable amount of work has been carried out on the subject of discrete nonlinear maps that exhibit deterministic chaos [1]. The possibility of interpreting amorphicity in solids as arising due to spatially chaotic atomic configurations was considered some years ago [2] by identifying them with the trajectories of a chaotic map such as the Baker map [1]. Such ideas have continued to attract the attention of several authors [3]. Needless to say, such studies would be all the more interesting and amenable to physical interpretation when the map concerned can be *derived* from a microscopic physical model in a systematic fashion. A well known example is the standard map [4]. This map can be obtained from the extremization condition on the energy of the Frenkel-Kontorova model [5] for a chain of interacting atoms adsorbed on a substrate: Its trajectories represent the extremum energy configurations [6] of the system.

In the field of magnetism, pioneering work carried out by Thompson *et al.* [7] showed that the planar states of the discrete anisotropic (*XYZ*) Heisenberg spin chain were time independent and could be spatially chaotic. It is clear that in analogy with the amorphicity of atomic configurations in solids mentioned in the beginning, such chaotic states would imply spin-glass-like configurations in the magnetic context. Around the same time, the presence of order and chaos in a classical *XY* spin chain was studied by Belobrov *et al.* [8] by analyzing the equilibrium spin configurations of the system. The above studies were in the *absence* of an external magnetic field. The *XY* anisotropy essentially played the role of the nonlinearity parameter in the respective maps obtained. Subsequently, a map describing planar states of the isotropic Heisenberg spin chain in the *presence* of an external, planar magnetic field was derived [9]. The advantage of such a study is that the external field provides a convenient, experimentally tunable nonlinearity parameter in the map. Preliminary results presented there showed that the map can support spatially chaotic spin configurations. As we shall show, the same map also arises in the case of the isotropic *XY* spin chain with a (symmetry breaking) external magnetic field *B* in the *x* direction. This is the model studied in this paper. Its Hamiltonian is given by [10,11]

$$H=-J\sum_i\ (S_i^xS_{i+1}^x+S_i^yS_{i+1}^y)-\mu B\sum_i\ S_i^x\,. \tag{1}$$

Here, in customary notation, J is a positive exchange constant for a ferromagnetic chain and μB is the field energy. In this model, the spin vectors $\mathbf{S}_i$ are constrained to rotate in the *XY* plane. Since $\mathbf{S}_i^2=S^2$ is a constant, we define $\mathbf{S}_i=(S_i^x,S_i^y)=S(\cos\phi_i,\sin\phi_i)$. The Hamiltonian in Eq. (1) can be then be written in units of JS^2 as

$$H=-\sum_i\ [\cos(\phi_{i+1}-\phi_i)+r\cos\phi_i], \tag{2}$$

where

$$r=\mu B/JS^2. \tag{3}$$

Thus the dimensionless parameter r is proportional to the external magnetic field *B*.

The statistical mechanics of this classical system was studied many years ago [12]. For $r=0$, the exact partition function can be found. For finite *r*, its high temperature behavior can be found perturbatively, by using the transfer matrix method [10]. More recently, certain nonlinear dynamical properties of this system have also been studied [11], with special reference to the connection with sine-Gordon soliton-like behavior for the excitations in the continuum version of

the model. Furthermore, Monte Carlo and molecular dynamics calculations have suggested [13] similarities between the discrete *XY* Hamiltonian [Eq. (1)] and $CsNiF_3$, a realistic ferromagnetic Heisenberg chain with a positive (easy-plane) anisotropy energy *D*, described by the Hamiltonian

$$H=-J\sum_i \mathbf{S}_i\cdot\mathbf{S}_{i+1}+D\sum_i (S_i^z)^2-\mu B\sum_i S_i^x, \qquad (4)$$

for certain parameter values.

The ground state of the *XY* spin chain in a field [Eq. (1)] is simple, i.e., it has all spins parallel to the *x* axis. The ground state energy is $-(1+r)$. At this point it is pertinent to mention that the ground states of a class of *canted XY* spin chains given essentially by the Hamiltonian $H=-\Sigma_i[\cos(\phi_{i+1}-\phi_i-\alpha)+r\cos p\phi_i]$, α being the canted-ness parameter, and *p* an integer, are more complicated and their phase diagrams have been studied in the literature [14]. But the behavior of the low-lying excitations, i.e., spin configurations with energy closest to the ground state energy has not been considered so far. In this paper, this is carried out for Eq. (2), an *uncanted* spin chain which is a special case of the above Hamiltonian, with $\alpha=0$ and $p=1$. As we shall see, even for this system with a simple ground state, the excitation energy displays a complex behavior as the parameter *r* (in this case, the magnetic field) is varied.

Our procedure is as follows: We first find all the equilibrium configurations by extremizing the energy [Eq. (1)] for a fixed field. We show that these configurations are described by the trajectories of a two-dimensional nonlinear map, which we call the spin map. We compute the energies of the members of the set of configurations of this map. From among them, we then identify the excitation with energy closest to the ground state for that field. This is repeated by varying the field. We then study the dependence of this lowest-energy excitation (measured with respect to the ground state) on the magnetic field. We show that sharp jumps in this energy occur at a primary critical field as well as at a hierarchy of several secondary critical magnetic fields at which the period of the spin configurations become commensurate with the natural period (i.e., unity) of the lattice. We interpret this result and analyze its physical implications on the behavior of the magnetization and the static susceptibility of the spin chain, highlighting the effect of both spatial chaos and field-induced transitions which are inherent in this system.

We begin by extremizing the energy of the *XY* Hamiltonian in Eq. (2) using $\partial H/\partial\phi_i=0$. This leads to

$$\sin(\phi_{i+1}-\phi_i)-\sin(\phi_i-\phi_{i-1})=r\sin\phi_i. \qquad (5)$$

Defining

$$\sin(\phi_{i+1}-\phi_i)=X_{i+1}, \qquad (6)$$

Eqs. (5) and (6) can be written as

$$X_{i+1}=X_i+r\sin\phi_i, \quad \phi_{i+1}=[\phi_i+\sin^{-1}X_{i+1}](\mathrm{mod}\ 2\pi). \qquad (7)$$

Here, $-1\leq X_i\leq 1$ and $0\leq\phi_i\leq 2\pi$. These equations represent a two-dimensional nonlinear map. We call this the spin map. As mentioned in the beginning, this map is identical to the map derived in an earlier paper [9] to describe the planar ($S_i^z=0$) states of a Heisenberg chain in a magnetic field. It is interesting to note that all planar states of $CsNiF_3$ and the *XY* chain [given by the Hamiltonians in Eq. (4) and Eq. (1), respectively] are necessarily time independent and are determined by the same spin map. For the former case, this is verified by considering the following dynamical equations arising from Eq. (4): On using $d\mathbf{S}_i/dt=[\mathbf{S}_i,H]$, where [,] denotes the Poisson bracket, we get

$$dS_i^x/dt=-J(S_{i-1}^y+S_{i+1}^y)S_i^z+J(S_{i-1}^z+S_{i+1}^z)S_i^y -D(S_i^zS_i^y+S_i^yS_i^z),$$

$$dS_i^y/dt=J(S_{i-1}^x+S_{i+1}^x)S_i^z-J(S_{i-1}^z+S_{i+1}^z)S_i^x+BS_i^z,$$

$$dS_i^z/dt=-J(S_{i-1}^x+S_{i+1}^x)S_i^y+J(S_{i-1}^y+S_{i+1}^y)S_i^x-BS_i^y.$$

On setting $S_i^z=0$ in the above equations, one obtains $dS_i^x/dt=dS_i^y/dt=dS_i^z/dt=0$, showing that these states are necessarily time independent. Furthermore, using $(S_i^x,S_i^y)=S(\cos\phi_i,\sin\phi_i)$ together with Eq. (6), it is readily seen that $dS_i^z/dt=0$ yields the map (7). (A similar argument holds good for the *XY* chain.)

In the spin map [Eq. (7)], the nonlinearity parameter is *r*. Thus for a fixed exchange interaction *J* this parameter can be tuned by changing the magnetic field *B* [see Eq. (3)]. The map has the following physical interpretation: Given the spin orientation ϕ_0 and ϕ_1 of the first two sites, which are the initial conditions, the map generates spin orientations at the rest of the sites. For some initial conditions and for nonzero values of *r*, i.e., the magnetic field, $|X_i|$ becomes greater than unity after a finite number of iterations. Since this is unphysical [see Eq. (6)], such initial conditions are not allowed in the phase space. Whether a given initial condition is allowed or not turns out to depend on *r* as well as the number of iterations *N*.

The paper is organized as follows: In Secs. II and III, we discuss some of the features of the spin map analytically: In particular, the ground state is shown to be the (dynamically) *unstable* fixed point of the map. We show that some of the numerical results on the change in behavior of the phase portraits with applied field can be understood by analyzing the map using a continuum approximation. Intriguingly, the discrete and continuum phase portraits look very similar for this system. In Sec. IV, the lowest-excitation energy, as well as the corresponding magnetization and the susceptibility for the lowest excitation are computed numerically as a function of the magnetic field. Section V contains the summary of our results and their physical interpretation.

II. THE SPIN MAP AND STABILITY OF FIXED POINTS

Before undertaking the numerical investigation of the spin map [Eq. (7)], let us understand some of its basic features analytically. For X_i very small the spin map reduces to the standard map [2]:

$$X_{i+1}=X_i+r\sin\phi_i, \qquad \phi_{i+1}=\phi_i+X_{i+1}. \qquad (8)$$

This is a well-studied map that exhibits chaos. It can also be verified that for small X_i, Eq. (2) reduces to the Frenkel-Kontorova Hamiltonian [5], on using Eq. (6).

The connection with a static sine-Gordon like configuration arises on writing Eq. (8) in the form $\phi_{i+1}-2\phi_i+\phi_{i-1}=r\sin\phi_i$. Then, making the continuum approximation $\phi_i\rightarrow\phi(\xi),\phi_{i\pm1}\rightarrow\phi(\xi\pm a)$, ($a$ being the nearest neighbor distance in the lattice), we get

$$a^2\phi_{\xi\xi}=r\sin\phi \tag{9}$$

with the well-known soliton (antisoliton) solution,

$$\phi(\xi)=4\tan^{-1}[\exp(\pm\sqrt{r}\xi/a)]. \tag{10}$$

The soliton solution interpolates between $\phi=0$ and $\phi=2\pi$ as $\xi\rightarrow\mp\infty$. Thus under the above approximations, the sine-Gordon soliton is present for *all* fields $r>0$. Furthermore, there is no possibility of chaotic configurations in this continuum approximation. This is because the continuum equation [Eq. (9)] has the same form as the equation of motion of a simple pendulum, on using the transformation $\phi\rightarrow(\phi+\pi)$, when ξ is identified with time. This is a one degree of freedom Hamiltonian system which is integrable by definition and hence cannot have chaotic solutions. As we shall see, these features will not be present in the discrete spin map [Eq. (7)], in the sense that, first, there is chaos and, second, the soliton disappears for large enough fields.

The properties of the spin map are quite different from that of the standard map. First, it is important to note that the $\sin^{-1}$ term, being multiple valued, gives rise to an ambiguity in the definition of the spin map. We remove this ambiguity by restricting the map to a specific branch of the $\sin^{-1}$ function, $-\pi/2\leqslant\sin^{-1}X_i\leqslant\pi/2$. This is justified since in the present paper our study is restricted to the low energy regime and as is clear from the structure of the Hamiltonian system, the second branch corresponds to higher energy than the branch selected for the r values considered in this paper.

It should be noted that since $\phi=0$ and $\phi=2\pi$ are identified, and $-1\leqslant X\leqslant1$, the spin map is defined on a cylinder of finite height. Next, we consider the stability of the fixed points of the spin map. Equations (2) and (6) show that the ground state of the model corresponds to $X_l=\phi_l=0$ for all l and the energy per site for the ground state is $-(1+r)$. The fixed points of the spin map are easily found to be (i) $X_l=0,\phi_l=0$ (the ground state) and (ii) $X_l=0,\phi_l=\pi$. The ''dynamical'' stability of the fixed points can be determined by finding the eigenvalues of the Jacobian matrix L_M given below, at the fixed points:

$$L_M=\begin{pmatrix}1 & r\cos\phi_l\\ \dfrac{1}{\sqrt{1-X_{l+1}^2}} & 1+\dfrac{r\cos\phi_l}{\sqrt{1-X_{l+1}^2}}\end{pmatrix}. \tag{11}$$

Since $\det L_M=1$, the map is area preserving. Eigenvalues of L_M are given by

$$\lambda_{1,2}=\frac{1}{2}[\mathrm{Tr}(L_M)\pm\sqrt{[\mathrm{Tr}(L_M)]^2-4}], \tag{12}$$

where

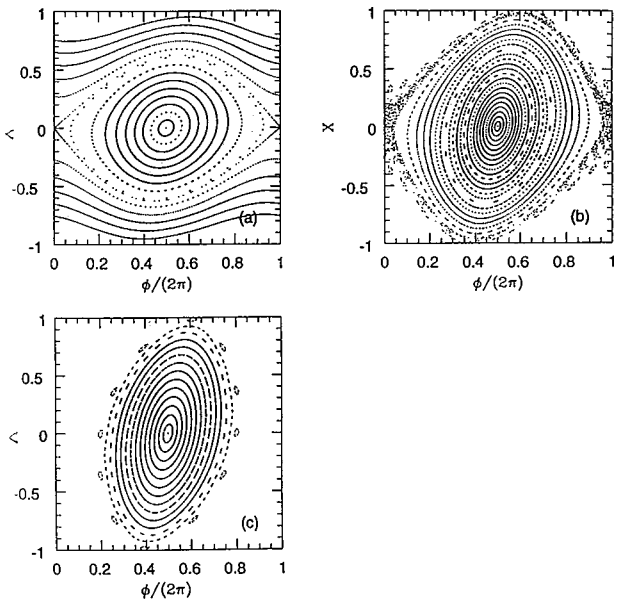

FIG. 1. Phase portrait of the spin map Eq. (7). (a) $r=0.1$; (b) $r=0.25$; (c) $r=0.38$.

$$\mathrm{Tr}(L_M)=2+\frac{r\cos\phi_l}{\sqrt{1-(X_l+r\sin\phi_l)^2}}. \tag{13}$$

As is well known, a fixed point is stable if the corresponding value of $|\mathrm{Tr}(L_M)|<2$ and unstable otherwise. For the ground state fixed point, $|\mathrm{Tr}(L_M)|=|2+r|$. Hence the ground state is an unstable fixed point for all positive r. On the other hand, the fixed point $X_l=0,\phi_l=\pi$ can be shown to be dynamically stable for all $r<4$. In this paper, we have presented results for $r<0.5$, since spatial chaos is most pronounced for small r.

III. SIMILARITIES BETWEEN THE DISCRETE AND CONTINUUM PHASE PORTRAITS

Generically, if a discrete map has complicated chaotic trajectories, studying its continuum version rarely gives any useful information about it. The logistic map and the standard map are typical examples [1]. For the spin map [Eq. (7)], in contrast, although the continuum version does miss all the 'local' intricacies of the trajectories, it turns out to be useful in the sense that it is able to predict analytically the primary critical field parameter r_c for which a global change in the *topology* of the allowed spin configurations takes place. In this section we discuss this intriguing feature of the spin map.

First we present the numerical results for the (ϕ,X) phase portraits of the discrete map. Figures 1(a), 1(b), and 1(c) correspond to three different r values ($r=0.1,0.25,0.38$). For a given r, each phase trajectory represents an extremum energy spin configuration. For $r=0.1$, three regions appear, with librational and rotational-type orbits, respectively. These regions are segregated by separatrixlike sets of points. As r increases the separatrix moves towards $X_i=\pm1$, respectively, and simultaneously starts to break down into chaotic orbits. The allowed phase space decreases with increase in r and so the phase space area covered by rotational orbits also

decreases. In other words, some rotational orbits become nonallowed and the chaotic region also increases. With further increase in r, more and more points in the chaotic regime become forbidden, till at a critical value of $r=r_c \simeq 0.26$, the main chaotic regime in the neighborhood of the hyperbolic fixed point disappears completely. Thus at r_c the ground state becomes disjoint from the rest of the allowed phase space. As r is increased beyond this, the chaotic regions in phase space diminish considerably. As the phase plot shrinks further, there appears a floating-island structure in the outermost region of the phase plot [see Fig. 1(c)]. The region around this island chain is nonallowed and this structure is disjoint from the rest of the allowed phase space. [We remark that in Fig. 1(c), the two curves just below the floating island chain are actually full curves but look broken, since we have not plotted all 5000 iterations for those initial conditions.] As already stressed, these features of the spin map are quite different from the standard map where the chaotic region keeps increasing with increase in the perturbation parameter and the full phase space is allowed for all values of the perturbation parameter. Further, such disjoint structures do not appear in the standard map.

Next we consider the following continuum equations derived analytically from Eq. (7):

$$\frac{d\phi}{d\xi}=\sin^{-1}X,$$
$$\frac{dX}{d\xi}=r\sin\phi. \tag{14}$$

(These would, of course, reduce to the sine-Gordon equation [Eq. (9)] on using the approximation $\sin^{-1}X \simeq X$). Equations (14) represents an integrable system of two coupled ordinary differential equations, with the following constant of motion E:

$$E=X\sin^{-1}X+\sqrt{1-X^2}+r\cos\phi. \tag{15}$$

The separatrix corresponds to $\phi=X=0$, giving $E_s=(1+r)$. Setting $E=E_s$ yields the following equation for the separatrix of Eq. (14):

$$X_s\sin^{-1}X_s+\sqrt{1-X_s^2}=1+2r\sin^2\phi_s/2. \tag{16}$$

The subscript s stands for the separatrix. It can be checked that the extremum value of $X_s=X_{max}$ corresponds to $\phi_s=\pi$. It is also easy to see that X_{max} increases with increase in r. To find the value of $r=r_c$ beyond which the separatrix becomes forbidden, we set $X_{max}=1$ and $\phi_s=\pi$ in the separatrix equation. This gives $r_c=\frac{1}{2}(\pi/2-1)\simeq 0.285$, which is quite close to our numerical result $r_c=0.26$ discussed in the beginning of this section.

The phase trajectories of the continuum equation [Eq. (14)] are given by expression Eq. (15) for E. Using this expression, the trajectories corresponding to different values of E are plotted in Figs. 2(a), 2(b), and 2(c), for $r=0.1$, $r=0.25$, and $r=0.38$, respectively. (Note that the outermost curves in these figures are actually not allowed, since their missing parts would lie in the forbidden region.) It is interesting to compare Fig. 2, the analytically found trajectories

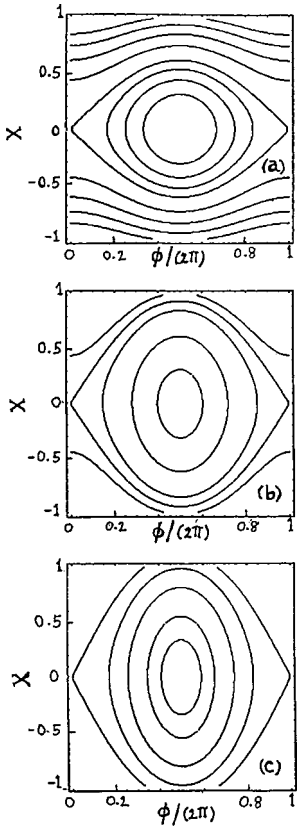

FIG. 2. Phase trajectories for the continuum version [Eq. (14)] of Eq. (7). (a) $r=0.1$; (b) $r=0.25$; (c) $r=0.38$.

in the continuum, with Fig. 1, the numerically found trajectories for the spin map [Eq. (7)], for the above values of r. Although there are nontrivial differences between Fig. 1 and Fig. 2, for example, there can be no chaos or floating islands in Fig. 2, nevertheless, a comparison of these figures shows that the overall shape and extent of the librational regions are very similar.

The physical message of the results of this section is as follows: For the XY spin chain with a field in the x direction, whose planar spin configurations are the orbits of the spin map [Eq. (7)], there exists a primary critical magnetic field $B_c=r_cJS^2/\mu$ [see Eq. (3)] beyond which the spin configurations spanning the full range of angles from $\phi=0$ to $\phi=2\pi$ (i.e., 2π soliton configurations) become forbidden. We have also shown an intriguing result that by merely analyzing the continuum version of the spin map, we are able to get a fairly accurate value of this critical field.

IV. FIELD DEPENDENCE OF EXCITATION ENERGY, MAGNETIZATION, AND SUSCEPTIBILITY

As already stated, the ground state energy per site of the system is easily found to be $-(1+r)$ analytically. We would like to compute the energy of the lowest excited state, i.e. the configuration with energy closest to the ground state energy. To find this numerically we systematically scan the full allowed phase space for each field r. But before stating those results, it turns out to be instructive to also find the *location* in phase space, of the trajectory corresponding to the lowest-energy excitation. As we shall see, this will help us interpret

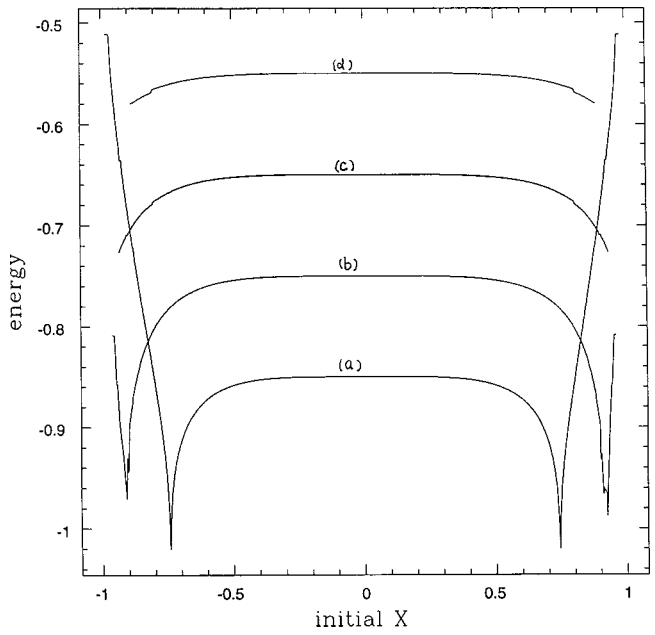

FIG. 3. Energy per site (in units of JS^2 versus initial conditions X on the symmetry line $\phi=\pi$. (*a*) $r=0.15$; (*b*) $r=0.25$; (*c*) $r=0.35$; (*d*) $r=0.45$.

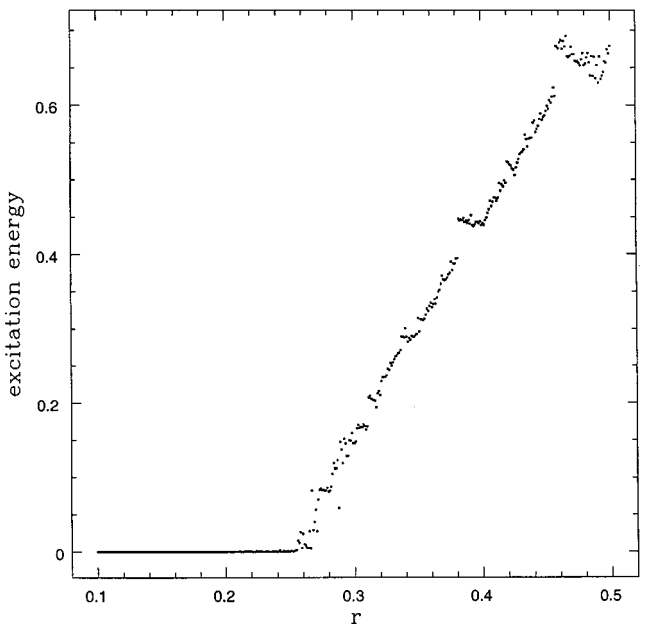

FIG. 4. Lowest-excitation energy per site (measured with respect to the ground-state energy per site, in units of JS^2) versus r.

our results. The following method suggested by Greene [15] proves to be useful for doing this. For a large class of maps it can be shown that there exist certain symmetry curves on which periodic orbits will lie generically. For the spin map these curves are $\phi=0$, $\phi=\pi$, and $X=\sin 2\phi$, as shown in the Appendix. We select initial conditions on a symmetry curve (e.g., $\phi=\pi$ would cover both rotational and librational orbits for all r) and iterate the map to find the corresponding spin configuration. For a given r, we then calculate the energy per site of each configuration by using Eq. (2).

Figure 3 reveals the following interesting behavior. On the x axis, we have the values of the different initial X selected on the symmetry curve $\phi=\pi$ in the phase space. Energy per site of the spin configurations corresponding to each of these initial conditions is plotted on the y axis. Four different values of r (0.15, 0.25, 0.35, and 0.45) have been chosen. For smaller r values, i.e., 0.15 and 0.25, there is a steep increase in the energy of the rotational and librational configurations close to, but on either side of, the separatrix as can be verified by comparing with the phase portraits in Fig. 1. In other words, there are cusps in the energy values at the separatrix. The separatrix corresponds to the lowest-energy configuration. The distance between the two cusps thus increases with r for $r \leqslant r_c$, as can be seen in Fig. 3. However, the separatrix would first break and finally disappear at around $r=r_c \simeq 0.26$ as seen in the previous section. Correspondingly, the cusps also first flatten, with a lot of fluctuations especially near 0.25 (due to increased chaos) and then disappear fully beyond r_c. For the larger r values (0.35 and 0.45) Fig. 3 shows that there are no cusps, and the spin configuration corresponding to the outermost trajectory of the allowed phase space has the lowest energy.

Interestingly the steady state behavior seems to influence the dynamical behavior of the system in a simple manner as can be seen from an earlier work [13]. There, the dynamics of the spin system has been studied using Monte Carlo simulations. It was found that the dynamical soliton disappears around $r=0.3$. This disappearance could not be understood in terms of the sine-Gordon approximation [11]. In contrast, this phenomenon can now be understood using the spin map which is more appropriate for the system. As we have seen, the steady-state soliton indeed disappears at $r=0.26$, which is quite close to the simulation estimate.

As mentioned in the beginning of this section, we now compute the energy more accurately, by scanning the full phase space for each r. We then plot the energy of the lowest-lying excitation (as measured from the ground state) as a function of the applied field r. This is given in Fig. 4. $N=5000$ as before. Here, excitation energy is measured with respect to the ground state energy $-(1+r)$. Note that jumps in the energy appear at certain critical values of r. The mechanism of these jumps is as follows. For all r values less than the primary critical field r_c, the value of the excitation energy is very close to the ground state energy. This is because although chaos sets in even for small r, the orbit corresponding to the lowest excitation continues to start and end in the region in the vicinity of the unstable fixed point (ground state). However, for $r=r_c$ the chaotic orbit surrounding the ground state becomes nonallowed and the location of the lowest-excitation orbit jumps (in phase space) to the outermost region of a central area. This leads to a sharp increase in the energy of the lowest excitation at r_c. As r is further increased, chaos gets reduced considerably. At a certain stage, the outermost region contains ''floating islands,'' which appears disjoint from the rest of the allowed phase space. With further gradual increase in r, the outer orbits of the islands start becoming nonallowed and at some point the lowest-excitation orbit becomes a commensurate configuration, where only the centers of the islands survive. This orbit appears disjoint from the rest of the allowed phase space. Just a little increase in r beyond this value makes this commensurate orbit nonallowed and thus its location once again has to make a jump in phase space to the outermost orbit of

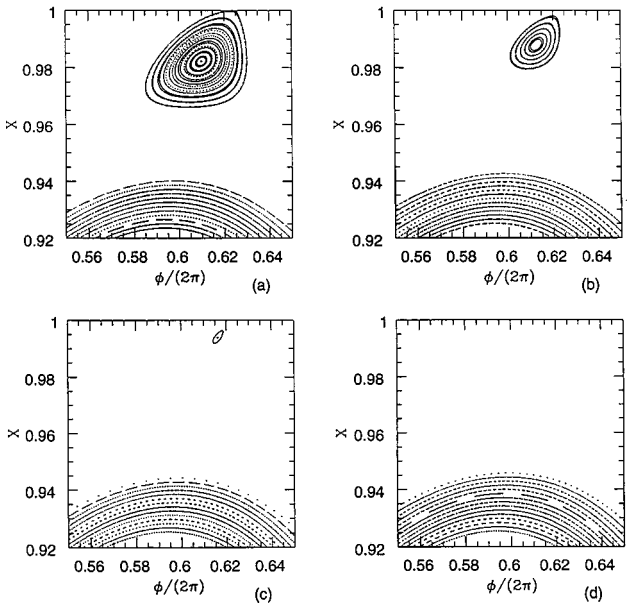

FIG. 5. Transition from a commensurate configuration associated with the energy jump at $r \simeq 0.38$ in Fig. 4: (a) $r=0.38$; (b) $r=0.381$; (c) $r=0.3817$; (d) $r=0.382$.

the (next) outermost island chain. This in turn causes a corresponding jump in the energy, and so on.

To understand this more clearly, we show in Fig. 5, the change in the phase-space structure corresponding to one such jump in energy found near $r \simeq 0.38$ in Fig. 4. Only a part of the phase space is shown to give a clearer picture. At $r=0.381$ there exists an island chain [Fig. 5(a)] which is disjoint from the central island and which contains the lowest excitation configuration. With increase in r [$r=0.381$, $r=0.3817$ in Figs. 5(b) and 5(c)], the island area decreases gradually till only the island center survives. Just beyond this, at $r=0.382$ [Fig. 5(d)] the island chain itself becomes nonallowed, and disappears, causing a jump is the position of the lowest excitation configuration from the disjoint island chain towards the central island. This in turn causes the jump in energy at this r value. This behavior keeps repeating. Thus energy increases sharply at all those secondary critical r values, when the lowest excitation becomes a (disjoint) commensurate configuration. The jump in the energy is a measure of the magnitude of the jump of the corresponding commensurate orbit in phase space at that critical field.

The physical manifestation of the above jumps that appear at and beyond r_c is best understood by computing the average magnetization $\langle S_x \rangle = 1/N \Sigma_i \cos \phi_i$ for the lowest-energy configurations. The plot of $\langle S_x \rangle$ as a function of r is given in Fig. 6. The magnetization takes on a constant maximal value (corresponding to that of the ground state) for all $r < r_c$. There is a sudden drop in the magnetization at the primary critical field $r = r_c = 0.26$ which also signals the disappearance of maximal chaos. There appear secondary minima in the magnetization at all the secondary critical fields where the energy jumps occurred.

In Fig. 7, the static susceptibility $\chi = \partial \langle S_x \rangle / \partial r$ is plotted as a function of r. χ is negligible for all $r < r_c$, but starts to fluctuate at the primary critical field. Thus the onset of fluctuations in χ can be regarded as the signature of the disappearance of the maximal spatial chaos in the phase space in this system. Fluctuations are also present at all the secondary fields when the spin configurations become commensurate, as described earlier.

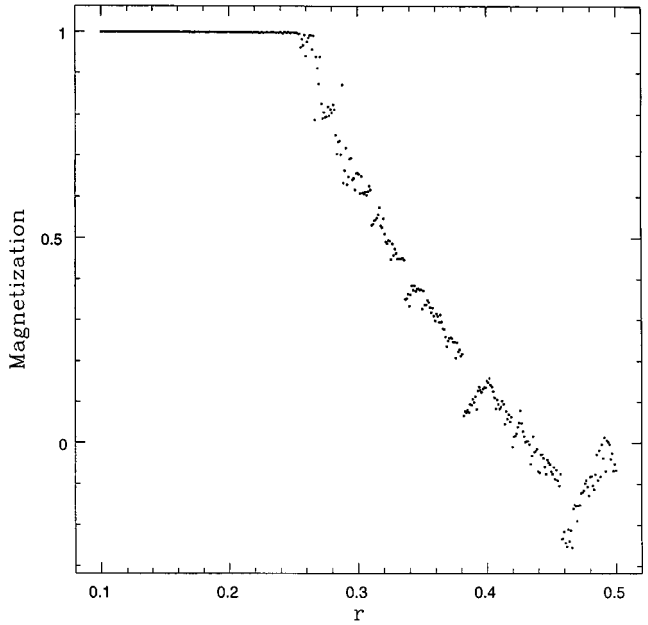

FIG. 6. Magnetization $\langle S_x \rangle$ (in arbitrary units) versus r.

V. SUMMARY AND PHYSICAL INTERPRETATION OF RESULTS

In this paper we have studied the change in the behavior of the spin configuration with energy closest to the ground state, for the *XY* spin chain as the applied external field along the x direction is varied. Physically, these configurations would be the relevant ones at sufficiently low temperatures. The results of such a study are amenable to experimental verification, since the magnetic field which essentially plays the role of the nonlinearity parameter, can be tuned easily.

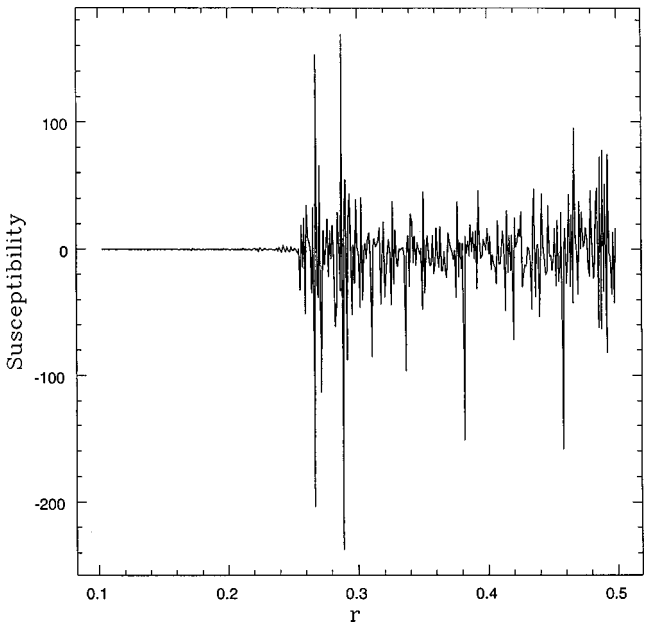

FIG. 7. Static susceptibility χ (in arbitrary units) versus r.

We have also investigated the effect on certain magnetic properties of the system. In particular, we have studied the susceptibility by retaining the underlying discreteness of the magnetic chain. We predict that there should be large fluctuations in the measured susceptibility at certain primary and successive secondary fields, arising due to the specific nonlinear effects inherent in this system.

Our results are summarized as follows: As is obvious, for any field, the ground state of the system has all the spins parallel to the x direction i.e., $\phi_i = 0(2\pi)$. We have shown that the extremal energy spin configurations for any field will be given by the spin map [Eq. (7)]. Since this is a two-dimensional map, given the initial spin orientations at the first two sites, the spin orientations at all the other sites can be found by iterating this map. This is first carried out for a fixed magnetic field, and we find the energy as well as the nature of the spin configuration that corresponds to the lowest-energy excitation above the ground state. This is then repeated for different magnetic fields. For very low fields, to a good approximation, the lowest-energy excitation is a 2π-soliton spin configuration on the lattice, where the spin orientation along the chain ranges from $\phi = 0$ to 2π in a regular fashion. As the field is increased, this excitation becomes a spatially chaotic orbit. Physically, this means that the soliton starts to get destabilized in the sense that while the spin configuration spans the full range of orientations from 0 to 2π, after a distance down the lattice, the successive spins point in a seemingly random fashion due to spatial chaos. Due to sensitivity to initial conditions, there are fluctuations in the energy, making it difficult to compute it in the chaotic regime.

With increase of the field, the chaotic region increases steadily till there is maximal chaos in the phase plot. Just beyond this, at a critical field, the ground state gets isolated from the orbit and chaos subsides considerably. The physical interpretation of this is that at this (primary) critical field, the lowest energy excitation spanning the full range 0 to 2π becomes forbidden, essentially because for the corresponding initial orientations, the iteration of the map leads to a complex angle of orientation at some successive site on the lattice. Further with this change of topology the lowest-energy excitation in the phase plot makes a finite jump to the outermost region of the (by now somewhat shrunk) allowed phase space. This region is composed of an elliptic chain of islands. This jump is shown to lead to a steep increase in the excitation energy at this critical field. As the field is increased further, the outer orbits of the islands start becoming forbidden due to the same reasons as given above. At a certain field, the excitation becomes a commensurate (periodic) configuration, which is seen to be disjoint from the rest of the allowed phase space. Hence with a very slight increase of field, at a secondary critical field, this commensurate orbit also becomes forbidden, and thus once again there is a finite jump in the location of the excitation orbit to the outermost region of the allowed phase space. This in turn leads to a sharp increase in the excitation energy, at this secondary field as well. This (secondary) behavior keeps repeating, giving way to a hierarchy of transitions between commensurate spin configurations to noncommensurate ones at corresponding critical field values. Each transition which causes the sharp increase in the excitation energy as seen in Fig. 4, is associated with a discontinuous change in the location of the lowest excitation orbit in the phase plot. The mechanism of such a jump in the energy near $r = 0.38$ in Fig. 4 can be clearly understood from Fig. 5. Physically, this implies that the character of the lowest-energy spin configuration changes abruptly from a periodic configuration at these critical fields. These phenomena in turn result in a hierarchy of jumps (gaps) in the graph of the excitation energy as a function of the field.

We wish to emphasize that although systems where the allowed phase space shrinks with a nonlinear parameter have been considered in the literature (Refs. [8], [[9], and [14]), the nontrivial change in the phase-space topology as it shrinks has not been reported earlier. Further we have shown here for the first time that there is a direct correlation between the changes in phase-space topology and jumps in the excitation energy that appear at certain special fields.

This complex behavior of the energy gives rise to a magnetization versus field plot (Fig. 6) which suggests a field-induced transition at the primary critical field r_c. Further, there are sharp minima in the magnetization at all the secondary critical fields. This in turn leads to the onset of fluctuations in the static susceptibility χ precisely at r_c as seen in Fig. 7, and can be regarded as an experimentally observable signal for the disappearance of maximal spatial chaos in the spin orientations. There are fluctuations in χ at all the secondary critical fields as well.

We parenthetically remark that the sine-Gordon approximation fails to describe the full nature of the *XY* spin chain. This is because this approximation not only misses the time evolution of the inherent chaotic spatial configurations, but more importantly, it *also* misses the change in topology of the phase plot (i.e., the disappearance of the soliton) at a certain critical field $r_c = 0.26$, which is inherent in the exact spin map. Recall that in contrast, for the sine-Gordon approximation of the map, the soliton persists for all fields. Now, simulations of the dynamics of a spin chain show the disappearance of the soliton around $r = 0.3$. As mentioned in existing literature (Refs. [11] and [13]) this phenomenon could not be understood using the sine-Gordon picture. From our present results this can be understood: We see that such a disappearance should indeed occur, since the correct description of the spin configurations of the chain is given by the spin map which in fact predicts this phenomenon. We have also shown that our estimate for r_c, which corresponds to the disappearance of the steady-state soliton is quite close to the field value for disappearance of a dynamical soliton, the computation of which is usually much more involved.

Soliton excitations in magnetic chains with different symmetries have been extensively studied [11], both theoretically and experimentally. In contrast, the possible physical manifestations of spatially chaotic spin configurations that are inherent in many magnetic chains have not received much attention. Although, to our knowledge, an *XY* spin chain has not been fabricated so far, this model and a realistic easy-plane ferromagnetic chain such as $CsNiF_3$ have been shown to possess identical behavior in the presence of a symmetry breaking field for some parameter values by earlier workers [11]. This connection is further substantiated by our results in Sec. IV where we have pointed out that the critical magnetic field at which a soliton disappears in the *XY*

spin map is very close to that at which a soliton disappears in Monte Carlo work [13].

Our theoretical results should motivate the fabrication of an *XY* spin chain, and we also suggest the following experiments and further theoretical work on this system: First, by using neutron scattering techniques at low temperatures and low fields, the static structure factor $S(k)$ should be found at a fixed field. Since the (isothermal) susceptibility is directly related to this factor [16], the experiment should be repeated for different finely tuned fields. One must then look for critical fields at which fluctuations in the susceptibility occur, and compare with Fig. 7. It would also be worthwhile to investigate whether similar results would appear in $CsNiF_3$, using experimental techniques that effectively probe only the planar states of this system, for which there is a close connection to the physics of the *XY* chain, as we have shown in Sec. I.

Second, the following extension of our theoretical study would give further insight into this nonlinear system that supports both order and chaos. Since there is an inherent self-similarity in the spin map (see Ref. [7]), it would be of interest to use renormalization group techniques, and investigate the possibility of predicting analytically, the successive critical fields at which the fluctuations in the susceptibility occur.

Third, the nature of the analogous low-energy configurations for a *canted XY* spin chain are also worth investigating, as a function of both the field and the cantedness parameter.

Finally, although chaos subsides for high fields for the system studied, it is worth studying if other observable effects such as the changes in the *symmetry* of the low-energy spin configurations can take place at such fields. Extension of this work to anisotropic spin chains is underway.

APPENDIX

Consider a class of area-preserving maps defined by

$$X_{i+1}=X_i+f_1(\phi_i),$$

$$\phi_{i+1}=\phi_i+f_2(X_{i+1}).$$

Let us symbolically denote this map by

$$T\begin{pmatrix} X_i \\ \phi_i \end{pmatrix}=\begin{pmatrix} X_{i+1} \\ \phi_{i+1} \end{pmatrix}. \tag{A1}$$

Provided f_1 is an odd function of ϕ, i.e., $f_1(-\phi_i)=-f_1(\phi_i)$, one can decompose T into the following two components $T=T_2T_1$ so that $T_1^2=T_2^2=I$ (I denotes the identity transformation), as follows:

$$T_1\begin{pmatrix} X \\ \phi \end{pmatrix}=\begin{pmatrix} X+f_1(\phi) \\ -\phi \end{pmatrix}, \tag{A2}$$

$$T_2\begin{pmatrix} X \\ \phi \end{pmatrix}=\begin{pmatrix} X \\ f_2(X)-\phi. \end{pmatrix}. \tag{A3}$$

It was shown by Greene [15] that when such a decomposition is possible, generically all the rational periodic orbits will have points on the fixed point curves of T_1 and T_2. Thus to compare the energy of two different rational orbits, instead of scanning the whole phase plane, one is required to scan only the symmetry curves defined by fixed points of T_1 and T_2. For the spin map Eq. (7), comparing with Eqs. (A1) and (A2), the symmetry curves are given by the following fixed points of T_1 and T_2, i.e.,

$$\phi=-\phi, \quad f_1(\phi)=r\sin\phi=0, \quad X=0,$$

$$f_2(X)=\sin^{-1}X=2\phi.$$

These yield the curves

$$\phi=0, \quad \phi=\pi, \quad X=0, \quad X=\sin 2\phi.$$

[1] See, for instance, A.J. Litchenberg and M.A. Lieberman, *Regular and Chaotic Motion* (Springer, Berlin, 1994).

[2] R. Schilling, Phys. Rev. Lett. **53**, 2258 (1984); P. Reichert and R. Schilling, Phys. Rev. B **30**, 917 (1984); **32**, 5731 (1985).

[3] J. Vollmer, W. Breymann, and R. Schilling, Phys. Rev. B **47**, 11 767 (1993); R.S. McKay and S. Aubry, Nonlinearity **7**, 1623 (1994); R. Livi, M. Spicci, and R.S. McKay, *ibid.* **10**, 1421 (1997).

[4] B.V. Chirikov, Phys. Rep. **52**, 265 (1979).

[5] T. Kontorova and Y.I. Frenkel, Zh. Eksp. Teor. Fiz. **8**, 89 (1938).

[6] S. Aubry, Phys. Rep. **103**, 127 (1984); P. Bak, Rep. Prog. Phys. **45**, 587 (1982).

[7] C.J. Thompson, K.A. Ross, B.J.P. Thompson, and M. Lakshmanan, Physica A **133**, 330 (1985).

[8] P.I. Belobrov, V.V. Beloshapkin, G.M. Zaslavskii, and A.G. Tret'yakov, Zh. Éksp. Teor. Fiz. **87**, 310 (1984) [Sov. Phys. JETP **60**, 180 (1984)].

[9] G. Ananthakrishna, Radha Balakrishnan, and Bai-lin Hao, Phys. Lett. A **121**, 407 (1987); **124**, 526(E) (1989).

[10] See, for example, D.C. Mattis, *The Theory of Magnetism* II (Springer, Berlin, 1984).

[11] H.J. Mikeska and M. Steiner, Adv. Phys. **40**, 191 (1991); **40**, 224 (1991); **40**, 313 (1991).

[12] M.E. Fisher, Am. J. Phys. **32**, 343 (1964).

[13] R.W. Gerling and D.P. Landau, Phys. Rev. B **37**, 6092 (1988); **41**, 7139 (1990).

[14] A. Banerjea and P.L. Taylor, Phys. Rev. B **30**, 6489 (1984); C.S.O. Yokoi, Lei-Han Tang, and Weiren Chou, *ibid.* **37**, 2173 (1988); Y. Fukui and T. Horiguchi, Physica A **199**, 580 (1993).

[15] J.M. Greene, J. Math. Phys. **20**, 1183 (1979).

[16] H.E. Stanley, *Phase Transitions and Critical Phenomena* (Clarendon Press, Oxford, 1971).